Letter

Acoustic spin-Chern topological Anderson insulators

Hui Liu,[1] Boyang Xie,[1] Haonan Wang,[1] Wenwei Liu,[1] Zhancheng Li ◉,[1] Hua Cheng,[1,*] Jianguo Tian,[1] Zhengyou Liu,[2,3,†]
and Shuqi Chen ◉[1,4,‡]

[1]*The Key Laboratory of Weak Light Nonlinear Photonics, Ministry of Education, Smart Sensing Interdisciplinary Science Center,
School of Physics and TEDA Institute of Applied Physics, Nankai University, Tianjin 300071, China*

[2]*Key Laboratory of Artificial Micro- and Nanostructures of Ministry of Education and School of Physics and Technology,
Wuhan University, Wuhan 430072, China*

[3]*Institute for Advanced Studies, Wuhan University, Wuhan 430072, China*

[4]*The Collaborative Innovation Center of Extreme Optics, Shanxi University, Taiyuan, Shanxi 030006, China*

Recent breakthroughs in topological Anderson insulators (TAIs) have revealed the counterintuitive possibility that sufficiently strong disorder can induce nontrivial topology from a trivial phase. Previous experimental research on TAIs has mainly focused on Chern-type and higher-order systems. However, the observation of spin-Chern-type TAI hosting disorder-induced spin-dependent boundary states remains unexplored. Here, we report on the experimental realization of a spin-Chern-type TAI in a two-dimensional bilayer phononic crystal. We directly observe evidence of TAI through disorder-induced pseudospin-dependent helical boundary modes from a trivial insulator and further demonstrate their robustness. By extending topological descriptions to disordered supercells and capturing the spin-Bott index, we confirm the topological Anderson phase transition. This work opens different perspectives for the realization of interesting topological phases in optics, circuits, and cold atom systems.

Introduction. Topological insulators (TIs) have been a topic of ongoing fascination in recent years due to their ability to support ideal propagation and their potential to revolutionize future devices. Topological gapless boundary states which arise from the nontrivial bulk topology of TIs have been observed in various systems, including condensed matter [1,2], optics [3–5], acoustics [6,7], mechanics [8,9], and cold atoms [10,11]. For TIs, their robustness against weak perturbations is at the heart of this topological phenomenon, but their robust transmission still cannot survive the destruction of strong disorder and is limited to an interesting phenomenon, known as Anderson localization [12–14]. However, recent research suggests that disorder may not always hinder topologically protected transmission, which has led to the proposal of topological Anderson insulators (TAIs) [15–18].

The discovery of TAIs can be traced back to the numerical research of disordered two-dimensional (2D) HgTe/CdTe quantum wells by Li *et al.* [15], which came as a surprise to the field of topological physics [19–22]. Simulated results showed a disorder-driven topological phase from a metallic phase. This novel quantum phase possesses a pair of disorder-induced helical edge states with opposite spins moving around the boundary in opposite directions, similar to a quantum spin Hall effect. Over the past decade, TAIs have attracted enormous interest and inspired extensive theoretical explorations in various topological systems, including spin-Chern-type [23–27] and Chern-type systems [28,29]. However, TAIs have been difficult to experimentally realize due to the lack of experimental schemes and real materials. To date, several TAIs have been observed in acoustic signals [30], cold atom wires [31], and photonic [32,33] and circuit systems [34], which are mainly limited to Chern-type and higher-order systems. Despite TAIs receiving considerable attention, a TAI with disorder-induced spin-dependent helical boundary states has yet to be reported experimentally.

In this Letter, we report the experimental realization of a spin-Chern-type TAI in a 2D bilayer phononic crystal. By introducing on-site energy disorder, we observed the emergence of a pair of pseudospin-dependent helical boundary states from a trivial phase, which is the hallmark of a spin-Chern-type TAI. We further demonstrated the topological properties of these disorder-induced boundary states, including their robust and pseudospin-dependent unidirectional propagations. Furthermore, we present evidence of a topological Anderson phase transition by extending topological descriptions to disordered systems. Our work offers a pathway to explore different disorder-driven topological phases and is expected to inspire further research in optics, circuits, and cold atom systems.

Model and methods. To illustrate the mechanism of a TAI in acoustic systems, we constructed a tight-binding model on a bilayer Lieb lattice. The supercell contains three types of atoms in each layer, denoted by A (red sphere), B (blue sphere), and C (green sphere), as shown in Fig. 1(a). The

---

*Corresponding author: hcheng@nankai.edu.cn

†Corresponding author: zyliu@whu.edu.cn

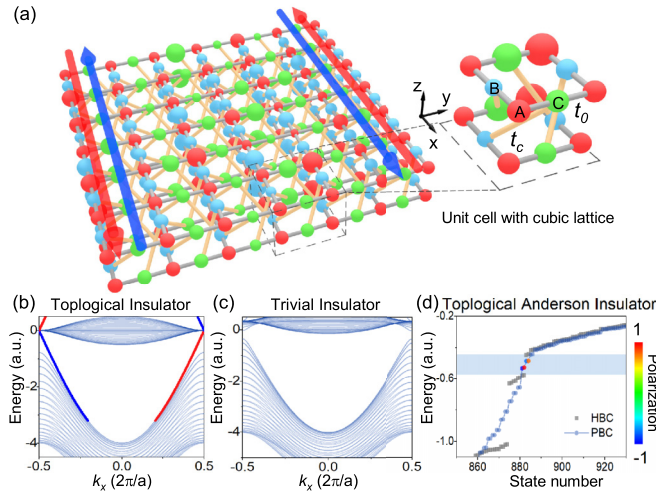‡Corresponding author: schen@nankai.edu.cn

FIG. 1. Spin-Chern TAI in a bilayer Lieb lattice model. (a) Schematic illustration of a TAI model in the presence of uniform on-site energy disorder. The inset shows one of the unit cells. (b) Band structure for TI by taking $t_0 = -2$, $t_c = -0.25$, and $m = 0$. (c) Band structure for the trivial insulator by increasing m to 0.35. (d) Calculated energy eigenvalues for TAI with an on-site energy disorder strength $w = 1$ in a 21×21 supercell with PBCs (gray dots) and HBCs (dark blue dots).

tight-binding Hamiltonian for the bilayer Lieb lattice model is given by

$$H = \sum_{i\in\{A,B,C\},\mu} U_{i,\mu} c_{i,\mu}^\dagger c_{i,\mu} + t_0 \sum_{\langle i,j\rangle,\mu} c_{i,\mu}^\dagger c_{j,\mu}$$
$$+ t_c \sum_{\langle\langle i,j\rangle\rangle,\mu} \{[\mu(\mathbf{n}_{ij}\cdot\mathbf{e}_z)+1]/2\} c_{i,\mu}^\dagger c_{j,-\mu}, \quad (1)$$

$$U_{i\in A;\mu} = -(m+U_{\text{dis}}), \quad U_{i\in B,C;\mu} = m+U_{\text{dis}}, \quad (2)$$

where $c_{i,\mu}^\dagger = (c_{i,1}^\dagger, c_{i,-1}^\dagger)$ are creation operators on the up/down layer at sites i. The first term is the on-site energy $U_{i,\mu}$, composed of an initial on-site energy m and on-site energy disorder U_{dis} for each atom. The second and the last term represent the nearest- and next-nearest-neighbor hopping, respectively. In these terms, $\langle i,j\rangle$ and $\langle\langle i,j\rangle\rangle$ run over all the nearest- and next-nearest-neighbor sites with hopping strengths t_0 and t_c, respectively. $\mathbf{n}_{ij} = \mathbf{e}_{ik} \times \mathbf{e}_{kj}$ denotes the unit vector connecting next-nearest-neighbor sites where k is the unique intermediate site between i and j. A schematic depiction of the TAI model is given in Fig. 1(a), where on-site disorder is introduced into each atom of a trivial supercell and represented by the size of the sphere. When on-site disorder is strong enough, this model exhibits the hallmark of a TAI, i.e., the emergence of disorder-induced boundary modes with pseudospin-up and pseudospin-down polarizations represented by red and blue arrows on the hard boundaries.

The construction of an acoustic topological Anderson phase can be qualitatively understood by the tight-binding model. This model is equivalent to a spin-Chern insulator for the disorder-free case ($U_{\text{dis}} = 0$) [7]. The layer pseudospin and chiral coupling provide synthetic spin-orbit coupling, leading to a nontrivial topology described by a nonzero spin-Chern number $C_s = 1$. The projected band structure is shown in

Fig. 1(b), where a pair of spin-momentum locking boundary states, denoted by red and blue lines, exist within the topological gap. When the initial on-site energy m increases, the effect of synthetic spin-orbit coupling is suppressed by a large on-site energy difference, forcing the system into a trivial phase ($C_s = 0$). The projected band structures are plotted in Fig. 1(c), where the gap is trivial and does not support any edge modes. However, an increase in on-site energy disorder can weaken the effect of the on-site energy difference, allowing the system to reenter the topological phase. We introduced random on-site energy disorder $U_{\text{dis}} = [-w/2, w/2]$ to each atom of the 21×21 supercell model, where w is the disorder strength. As the disorder strength increases to 1, a trivial gap may close and a nontrivial gap may open, as shown in Fig. 1(d). The eigenenergy of the supercell with periodic boundary conditions (PBCs) presents a gap, denoted by the blue area. The energy spectrum with hard boundary conditions (HBCs) confirms the disorder-induced phase transition, characterized by the occurrence of pairs of topological edge modes within the gap region. Similarly, introducing disorder into the chiral coupling can enhance synthetic spin-orbit coupling and lead to a TAI. However, a TAI cannot be driven by disordered types that cannot cause topological phase transitions, such as in-plane coupling t_0. Further details can be found in Supplemental Material (SM) Notes 1 and 2 [35].

To identify the nontrivial topology in a TAI without a well-defined band structure, we extend the topological description to real space and capture the topological invariant using the spin-Bott index. We introduce a pseudospin operator $\tau_\mu = \sigma_\mu \otimes I_N$, where the Pauli matrices σ_μ act as the layer degree of freedom and N is the number for one-intralayer atoms. The Hamiltonian of the supercell can be expressed as a block matrix by setting PBCs, which allows us to extract the synthetic spin-orbit coupling and the spin-mixing term contributed by the chiral coupling. Owing to the existence of the spin-mixing term, τ_μ is not commutative with H, indicating the pseudospin nonconservation of the system. Nevertheless, we can define a pseudospin space of σ_y based on the layer and split the bulk states below the gap into pseudospin-up and pseudospin-down groups by projection, as long as the spin-mixing term is not large (see SM Note 3 for details [35]). The split pseudospin-dependent groups allow us to obtain the spin-Bott index, which describes the topological properties of the supercell. As the spin-Bott index does not depend on any symmetries and pseudospin conservation, it is an effective tool for measuring topology based on real space. Similar to the spin-Chern number, the spin-Bott index relies on the presence of both a complete bulk gap and a spin-projection gap. Details of the spin-Bott index calculation are provided in SM Note 4 [35].

To transplant from the tight-binding model to a concrete acoustic structure, we need to find a unit geometry where the variation of on-site energy satisfies the formation mechanism of a TAI. The unit cell with a bilayer Lieb lattice is shown in Fig. 2(a), where square scatterers with width $l = 14.4$ mm and height $h_1 = 8.4$ mm create a Lieb lattice at each layer. The interlayer couplings that connect two air layers are realized by four chiral tubes with diameter $d = 3.3$ mm and height $h_2 = 9.6$ mm. The square unit cell hosts the lattice constant $a = 24$ mm and total height $h = 26.4$ mm. The top view of the unit structure is shown in the inset, where square scatterers
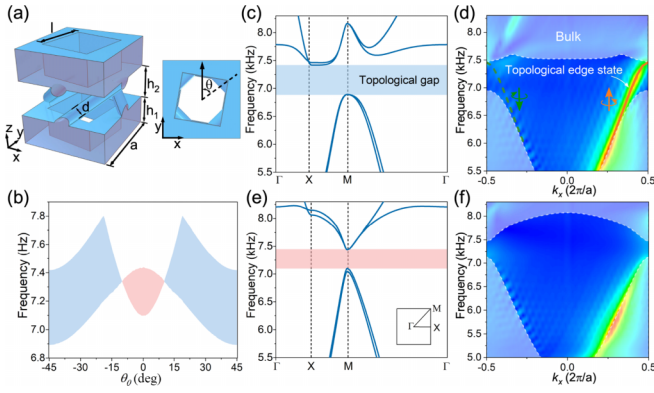
FIG. 2. Structural implementation of acoustic spin-Chern TAI and the band structure for two disorder-free phases. (a) Unit cell of an acoustic TAI, composed of two air layers with scatterers and four chiral tubes. The inset shows the top view of the TAI cell structure with scatterers rotating at random angles uniformly distributed between $\theta_0 - \theta_d/2$ and $\theta_0 + \theta_d/2$. Air fills the entire blue area. (b) The complete gap of the disorder-free unit cell is represented as a function of θ_0. (c) The bulk band structure and (d) the projected band dispersions for a TI with $\theta_0 = \pm 45°$ and $\theta_d = 0°$. (e) The bulk band structure and (f) the projected band dispersions for a trivial insulator with $\theta_0 = 0°$ and $\theta_d = 0°$.

with hard boundaries in the upper and lower air layers rotate simultaneously. The rotation angles between the diagonal of the square scatterers and the y direction are defined as $\theta = \theta_0 + \theta_d R$, where θ_0 is the initial rotation angle, θ_d is the modulation parameter representing disorder strength, and R is a random number with a uniform distribution within $[-0.5, 0.5]$ applied independently to each unit cell. Although the rotation of the scatterers changes all the in-plane parameters, including the on-site energy and the in-plane coupling, only the modulation of on-site energy leads to a topological phase transition. In the structure design, we mainly rely on two key ingredients: synthetic spin-orbit coupling induced by a bilayer lattice and chiral air tubes, and on-site energy modulated by rotating square scatterers.

The formation of TAI requires two distinct phases. The topological phase is ensured by the synthetic spin-orbit coupling. The trivial phase occurs when the spin-orbit coupling is covered by the on-site energy difference introduced by the initial rotation angle θ_0 of the scatterers. For the disorder-free case ($\theta_d = 0$), we focus on a complete gap between the first/second and third/fourth bands of the system. Figure 2(b) shows the simulated complete gap as a function of θ_0, where a topological gap ($C_s = 1$) denoted by the pink area closes and a trivial gap ($C_s = 0$) denoted by the blue areas opens, as the rotation of θ_0 from $-45°$ to $0°$ increases the on-site energy difference. The gap closes at $\theta_0 = \pm 10.5°$, indicating a phase transition and band inversion. Since the on-site energy in the real acoustic structure cannot achieve infinite change without destroying the lattice, the on-site energy in the TAI structure is designed to change only within a certain range. Thus, as θ_0 further increases from $0°$ to $45°$, the on-site energy decreases, and the system returns to the topological phase. The rotation of the scatterers with θ_0 changes both the on-site energy difference and the in-plane coupling, ensuring a topological phase

transition and a complete gap, respectively. The topological properties of these distinct phases can be further investigated by the band structures with specific initial rotation angles. For a topological phase with $\theta_0 = \pm 45°$, the simulated bulk band structure along high-symmetry lines is displayed in Fig. 2(c). A double Dirac cone at point M opens and a completely topological band gap denoted by the blue area arises, owing to the chiral interlayer coupling and minimum on-site energy difference. The relevant projected band dispersions along k_x are shown in Fig. 2(d), with the experimental dispersion obtained by a Fourier transform in color maps and simulated results in overlaid lines. A pair of boundary states with the pseudospin-up and psueodspin-down polarization exist in the topological gap, represented by orange and green lines. The pseudospin-up polarized boundary state is experimentally excited and agrees well with the simulation. When $\theta_0 = 10.5°$, the increasing on-site energy difference counteracts the effect of the synthetic spin-orbit coupling, closing the topological band gap and creating a double Dirac cone occurs at point M. For the trivial case with $\theta_0 = 0°$, the maximum on-site energy difference opens a trivial gap indicated by the pink area in Fig. 2(e). The projected band dispersions in Fig. 2(f) show a complete trivial band gap without any modes. Starting from this trivial phase, we will demonstrate how a global change in the on-site energy difference can induce a topological phase transition by disorder.

Experimental realization in a phononic crystal. The three-dimensional (3D) printed TAI sample with 21×21 unit cells consists of a bilayer Lieb lattice with rotated scatterers and interlayer chiral air tubes, as shown in Fig. 3(a). More details about the experimental setup and TAI sample can be found in SM Note 5 [35]. By increasing the disorder strength θ_d, the on-site energy difference can be weakened and the trivial phase can transform into the topological regime. An Anderson phase diagram as a function of the initial angle θ_0 and disorder strength θ_d is given in Fig. 3(b), where each data point is the average of the spin-Bott index for more than ten acoustic supercells with 11×11 unit cells. This average phase diagram shows the general phase transition trend, that is, strong enough disorder can take the system from the trivial phase (pink area) to the topological phase (blue area). However, it cannot bring the system back to the trivial phase because the disorder introduced by rotated scatterers cannot indefinitely increase. This phase diagram provides evidence for the existence of a TAI.

We further investigate the process of a disorder-induced phase transition, denoted by the green arrow in Fig. 3(b), by observing the appearance of a pair of disorder-induced edge states in a TAI sample with 21×21 unit cells. The topological Anderson phase driven by random rotating scatterers arises from an on-site energy disorder varying within a certain range (see SM Note 6 for more details [35]). The TAI sample was fabricated by applying sufficiently strong disorder $\theta_d = 180°$ to a trivial phase with initial rotation angle $\theta_0 = 0°$ in Figs. 2(e) and 2(f). The simulated eigenfrequencies of the TAI sample with PBCs and HBCs are displayed in Fig. 3(c). The energy spectrum with PBCs has a topological gap (7166–7561 Hz) denoted by the blue area. Several pairs of boundary states exist within the gap region of the energy spectrum with HBCs, indicating that the nontrivial topological properties are driven from the trivial phase by disorder. The pseudospin
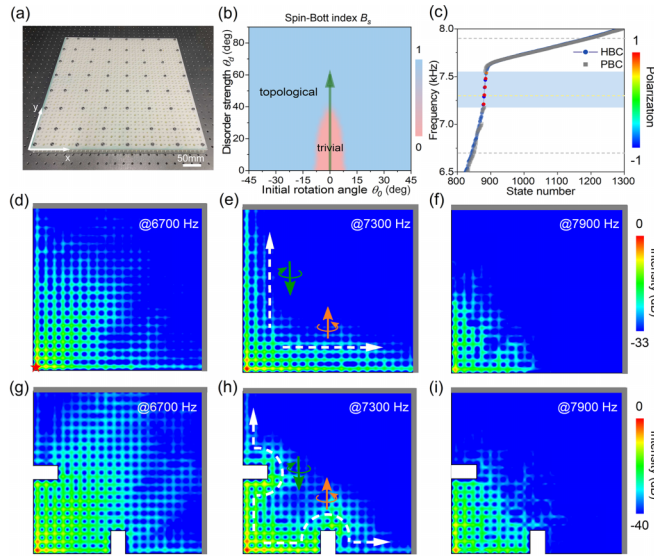
FIG. 3. Topological Anderson phase and disorder-induced pseudospin-dependent helical boundary modes. (a) A photograph of the TAI sample with $\theta_0 = 0°$ and $\theta_d = 180°$. The small holes in the upper layer are reserved for measurement, and the cylindrical holes outside the structure are used to hold the sample. (b) Simulated TAI phase diagram as a function of θ_0 and θ_d simulated in supercells with 11×11 unit cells. (c) Simulated eigenfrequency for the TAI sample with 21×21 unit cells in the presence of PBCs (gray dots) and HBCs (dark blue dots). The red and blue in the color map denote pseudospin up and pseudospin down, respectively. (d)–(f) Experimental acoustic fields of the TAI sample excited at 6700, 7300, and 7900 Hz, mapping to a bulk mode, boundary modes, and a bulk mode, respectively. A pair of boundary modes at the gap frequency, denoted by the orange and green arrows, respectively, propagate in different directions along two hard boundaries. (g)–(i) Experimental acoustic fields of a TAI transmitted around obstacles. The gray lines represent open boundaries and the others are hard boundaries.

polarization of the boundary eigenmodes, determined by projecting eigenmodes into pseudospin space, is represented by a color map. The emergence of pseudospin-dependent helical boundary states, as another key hallmark of a TAI, can be observed with midgap excitation at hard boundaries in the sample.

We measured an acoustic pressure field excited at the junction of two hard boundaries in the x and y directions. The results at typical frequencies are shown in Figs. 3(d)–3(f). The acoustic pressure intensity radiates from the excitation source to the interior at frequencies of 6700 and 7900 Hz, showing bulk mode distribution. At a gap frequency of 7300 Hz, the field distribution supports transmissions along the two hard boundaries, indicating that the on-site energy disorder weakens the on-site energy difference of the initial trivial phase and induces a pair of boundary states from a trivial phase. As the sound intensity decays away from the boundary, it displays a characteristic behavior of boundary modes. More details about their pseudospin polarization, which carries pseudospin up (orange arrow) along the x direction and pseudospin down (green arrow) along the y direction, can be found in SM Note 7 [35]. Figures 3(g)–3(i) demonstrate the robustness of the disorder-induced pseudospin-dependent boundary state against a rectangular defect. At a midgap frequency of 7300 Hz, the intensity of the acoustic field is distributed at the hard boundary and smoothly propagates around the defect, where backscattering is apparently suppressed. These experimental results demonstrate the existence of pseudospin-dependent boundary states in TAI samples, similar to those in a TI.

Conclusions. In summary, we have observed a spin-Chern-type TAI in a 2D acoustic system with bosonic time-reversal symmetry. This TAI is characterized by topological spin-dependent helical boundary states driven by disorder. The transition from a trivial phase to a disorder-driven topological phase has been verified both qualitatively and quantitatively through the observation of disorder-induced helical boundary states and the emergence of a topological Anderson phase transition characterized by the spin-Bott index. Moreover, the disorder-induced boundary states have been experimentally proved to be immune to obstacles. Our work differs from earlier studies on TAIs in several ways. First, we experimentally realize a spin-Chern-type TAI, leading to the observation of a disordered-induced quantum spin-Hall-like effect. Second, we experimentally demonstrate that topological Anderson phases can exist without pseudospin conservation and any symmetries. Third, our experiments are conducted in an acoustic system with bosonic time-reversal symmetry, expanding the implementation platform of spin-Chern-type TAIs, which may encourage research and applications of topological phases in other platforms.

[1] M. Z. Hasan and C. L. Kane, Colloquium: Topological insulators, Rev. Mod. Phys. **82**, 3045 (2010).

[2] X.-L. Qi and S.-C. Zhang, Topological insulators and superconductors, Rev. Mod. Phys. **83**, 1057 (2011).

[3] F. D. M. Haldane and S. Raghu, Possible realization of directional optical waveguides in photonic crystals with broken time-reversal symmetry, Phys. Rev. Lett. **100**, 013904 (2008).

[4] L. Lu, J. D. Joannopoulos, and M. Soljačić, Topological states in photonic systems, Nat. Phys. **12**, 626 (2016).

[5] Y. Yang, Z. Gao, H. Xue, L. Zhang, M. He, Z. Yang, R. Singh, Y. Chong, B. Zhang, and H. Chen, Realization of a three-dimensional photonic topological insulator, Nature (London) **565**, 622 (2019).

[6] Z. Yang, F. Gao, X. Shi, X. Lin, Z. Gao, Y. Chong, and B. Zhang, Topological acoustics, Phys. Rev. Lett. **114**, 114301 (2015).

[7] W. Deng, X. Huang, J. Lu, V. Peri, F. Li, S. D. Huber, and Z. Liu, Acoustic spin-Chern insulator induced by synthetic

spin–orbit coupling with spin conservation breaking, Nat. Commun. **11**, 3227 (2020).

[8] S. D. Huber, Topological mechanics, Nat. Phys. **12**, 621 (2016).

[9] D. Rocklin, S. Zhou, K. Sun, and X. Mao, Transformable topological mechanical metamaterials, Nat. Commun. **8**, 14201 (2017).

[10] G. Jotzu, M. Messer, R. Desbuquois, M. Lebrat, T. Uehlinger, D. Greif, and T. Esslinger, Experimental realization of the topological haldane model with ultracold fermions, Nature (London) **515**, 237 (2014).

[11] M. Aidelsburger, M. Lohse, C. Schweizer, M. Atala, J. T. Barreiro, S. Nascimbène, N. Cooper, I. Bloch, and N. Goldman, Measuring the Chern number of Hofstadter bands with ultracold bosonic atoms, Nat. Phys. **11**, 162 (2015).

[12] P. W. Anderson, Absence of diffusion in certain random lattices, Phys. Rev. **109**, 1492 (1958).

[13] M. Segev, Y. Silberberg, and D. N. Christodoulides, Anderson localization of light, Nat. Photonics **7**, 197 (2013).

[14] Y. Ye, M. Ke, J. Feng, M. Wang, C. Qiu, and Z. Liu, Transversal Anderson localization of sound in acoustic waveguide arrays, J. Phys.: Condens. Matter **27**, 155402 (2015).

[15] J. Li, R.-L. Chu, J. K. Jain, and S.-Q. Shen, Topological Anderson insulator, Phys. Rev. Lett. **102**, 136806 (2009).

[16] C. W. Groth, M. Wimmer, A. R. Akhmerov, J. Tworzydło, and C. W. J. Beenakker, Theory of the topological anderson insulator, Phys. Rev. Lett. **103**, 196805 (2009).

[17] A. Yamakage, K. Nomura, K.-I. Imura, and Y. Kuramoto, Disorder-induced multiple transition involving Z_2 topological insulator, J. Phys. Soc. Jpn. **80**, 053703 (2011).

[18] Y. Xing, L. Zhang, and J. Wang, Topological Anderson insulator phenomena, Phys. Rev. B **84**, 035110 (2011).

[19] E. Prodan, Three-dimensional phase diagram of disordered HgTe/CdTe quantum spin-Hall wells, Phys. Rev. B **83**, 195119 (2011).

[20] L. Chen, Q. Liu, X. Lin, X. Zhang, and X. Jiang, Disorder dependence of helical edge states in HgTe/CdTe quantum wells, New J. Phys. **14**, 043028 (2012).

[21] H. Jiang, L. Wang, Q.-F. Sun, and X. C. Xie, Numerical study of the topological Anderson insulator in HgTe/CdTe quantum wells, Phys. Rev. B **80**, 165316 (2009).

[22] Y.-Y. Zhang, R.-L. Chu, F.-C. Zhang, and S.-Q. Shen, Localization and mobility gap in the topological Anderson insulator, Phys. Rev. B **85**, 035107 (2012).

[23] Z.-Q. Zhang, B.-L. Wu, J. Song, and H. Jiang, Topological Anderson insulator in electric circuits, Phys. Rev. B **100**, 184202 (2019).

[24] V. Adak, K. Roychowdhury, and S. Das, Spin Berry phase in a helical edge state: S_z nonconservation and transport signatures, Phys. Rev. B **102**, 035423 (2020).

[25] R. Shindou and S. Murakami, Effects of disorder in three-dimensional Z_2 quantum spin Hall systems, Phys. Rev. B **79**, 045321 (2009).

[26] H.-M. Guo, G. Rosenberg, G. Refael, and M. Franz, Topological Anderson insulator in three dimensions, Phys. Rev. Lett. **105**, 216601 (2010).

[27] X. Cui, R.-Y. Zhang, Z.-Q. Zhang, and C. T. Chan, Photonic Z_2 topological Anderson insulators, Phys. Rev. Lett. **129**, 043902 (2022).

[28] P. Titum, N. H. Lindner, and G. Refael, Disorder-induced transitions in resonantly driven Floquet topological insulators, Phys. Rev. B **96**, 054207 (2017).

[29] P. Titum, N. H. Lindner, M. C. Rechtsman, and G. Refael, Disorder-induced Floquet topological insulators, Phys. Rev. Lett. **114**, 056801 (2015).

[30] F. Zangeneh-Nejad and R. Fleury, Disorder-induced signal filtering with topological metamaterials, Adv. Mater. **32**, 2001034 (2020).

[31] E. J. Meier, F. A. An, A. Dauphin, M. Maffei, P. Massignan, T. L. Hughes, and B. Gadway, Observation of the topological anderson insulator in disordered atomic wires, Science **362**, 929 (2018).

[32] S. Stützer, Y. Plotnik, Y. Lumer, P. Titum, N. H. Lindner, M. Segev, M. C. Rechtsman, and A. Szameit, Photonic topological Anderson insulators, Nature (London) **560**, 461 (2018).

[33] G.-G. Liu, Y. Yang, X. Ren, H. Xue, X. Lin, Y.-H. Hu, H.-X. Sun, B. Peng, P. Zhou, Y. Chong, and B. Zhang, Topological Anderson insulator in disordered photonic crystals, Phys. Rev. Lett. **125**, 133603 (2020).

[34] W. Zhang, D. Zou, Q. Pei, W. He, J. Bao, H. Sun, and X. Zhang, Experimental observation of higher-order topological Anderson insulators, Phys. Rev. Lett. **126**, 146802 (2021).

[35] See Supplemental Material at http://link.aps.org/supplemental/10.1103/PhysRevB.108.L161410 for detailed descriptions of the analysis of the disordered types for TAI, the topological descriptions of the disorder system, the calculation of the spin-Bott index, and characteristics of disorder-induced helical boundary states, which includes Refs. [36–40].

[36] T. A. Loring and M. B. Hastings, Disordered topological insulators via C*-algebras, Europhys. Lett. **92**, 67004 (2011).

[37] T. A. Loring, Quantitative K-theory related to spin Chern numbers, SIGMA **10**, 077 (2014).

[38] D. Toniolo, Time-dependent topological systems: A study of the Bott index, Phys. Rev. B **98**, 235425 (2018).

[39] H. Huang and F. Liu, Quantum spin Hall effect and spin Bott index in a quasicrystal lattice, Phys. Rev. Lett. **121**, 126401 (2018).

[40] H. Huang and F. Liu, Theory of spin Bott index for quantum spin Hall states in nonperiodic systems, Phys. Rev. B **98**, 125130 (2018).